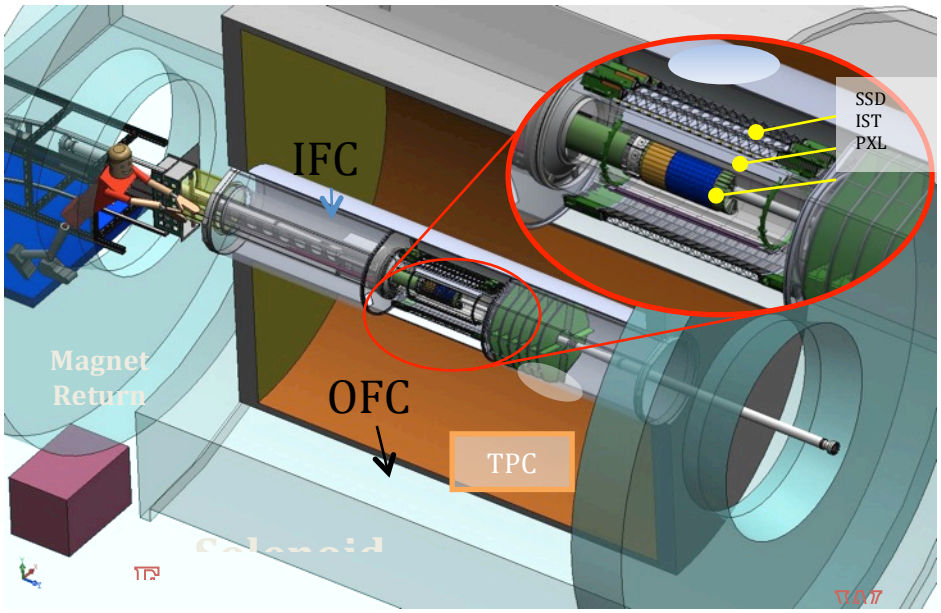

REPORT ON VERIFICATION OF KEY PERFORMANCE PARAMETERS

July 16, 2014

Performing Organization Location:	Brookhaven Science Associates Brookhaven National Laboratory Upton, New York 11973-5000
Contract Period of Performance	FY2010-FY2015

BROOKHAVEN NATIONAL LABORATORY

Executive Summary

The document describes in detail how the HFT Key Performance Parameters are met. Table 1 shows the KPPs from the PEP. In short, all of the Key Performance Parameters have been met.

Parameter	Threshold value	Optimal value	Value achieved	
Pointing resolution of HFT system (750 MeV/c kaons)	≤60 μm in the r-phi plane and Z	~45 μm in r-phi plane and Z	55 μm	Met
Single-track efficiency for HFT system, requiring PXL hits on both layers. (1 GeV/c pions)	≥ 60%	≥ 75%	65%	Met
Compatible with STAR DAQ-1000 system	<20% dead time from HFT system at 1kHz	<15% dead time from HFT system at 1kHz.	~0% for PXl, IST. 16% for SSD	Met

Table 1 : Key Performance Parameters and values achieved

A detailed documentation of the demonstration of the KPP is in the following sections of this document. In brief:

- The pointing resolution has been extracted from Au+Au 200 GeV collision data using the TPC-IST-PXL subsystem. The tracking required a hit (point) on the two layers of PXL and on the IST. The DCA was measured as a function of the momentum p and azimuthal angle ϕ for particles identified using TOF and dE/dx from the TPC. An overall value of 55 μm was achieved for 750 MeV/c kaons. The analysis indicates that for the two sectors where inner ladders are built using the Al-based cable, a value close to the optimal value has been achieved. The observed dependence on momentum is consistent with simulations.
- A complete description of the HFT detector was developed with the as-built dimensions and material budget. The single-track efficiency was calculated using the full STAR simulation package. The analysis was carried out for Minimum Bias events including pile-up and an efficiency of 65% was achieved using the current official tracking that is yet to be optimized.

- The complete HFT system is read out by the STAR DAQ system. The dead times for PXL and IST are at or below the TPX dead time, so NO additional dead time is imposed on the readout due to the inclusion of these two detector. The hybrids on the old SSD ladders have an intrinsic busy of 160 microseconds, so the ultimate achievable dead time will be 15% at a requested trigger rate of 1 kHz.

Introduction

A prerequisite to obtain CD-4 for the HFT is to verify that the system can achieve the three Key Performance Parameters (KPP) listed in the Project Execution Plan (PEP). In the following paragraphs, we first outline these requirements as agreed and presented in the PEP, and then we present the data (real and/or simulations) and methods used to obtain performance results of the HFT system that demonstrate the compliance with the requirements.

Key Performance Parameter requirements for the HFT system (from PEP)

The following text, in italics, is a straight copy of the relevant excerpts in the PEP.

The HFT key performance parameters (KPPs) are given in Table 2-1 of the PEP. The capability of the HFT system to achieve the KPPs will be demonstrated through the measurement of subsystem functional parameters and detailed, realistic simulations using the full STAR detector simulation package and analysis software. The subsystem functional parameters will be obtained through bench tests, survey measurements, and the meeting of design specifications. The planned early finish schedule (see Section 2.3) has the HFT system ready for installation into STAR approximately two months prior to the Run-14 start date (approximately December 2013). As verification of the KPPs with beam is preferred, the project will attempt to demonstrate these using RHIC Run-14 Au-Au collision data. Appendix A provides further details on the KPPs and the underlying subsystem functional parameters.

Parameter	*Threshold value*	*Optimal value*
Pointing resolution of HFT system (750 MeV/c kaons)	*≤60 μm in the r-phi plane and Z*	*~45 μm in r-phi plane and Z*
Single-track efficiency for HFT system, requiring PXL hits on both layers. (1 GeV/c pions)	*≥ 60%*	*≥ 75%*
Compatible with STAR DAQ-1000 system	*<20% dead time from HFT system at 1kHz*	*<15% dead time from HFT system at 1kHz.*

Table 2-1 CD-4 key performance parameters

CD-4 Key Performance Parameters

The instrument must be capable of a pointing resolution in r-phi of better than 60 μm for kaons of 750 MeV/c. 750 MeV/c is the mean momentum of the decay kaons from D^0 mesons of 1 GeV/c transverse momentum, the expected mean of the D meson distribution. The pointing resolution is defined as the width of a Gaussian fit (in sigma) to the distribution of distance of closest approach vectors (DCA) in the X-Y plane to the primary event vertex in 0-5% central Au-Au collisions. The pointing resolution in z will be similar. The resolution in z is defined as the square root of the difference between the squared 3D DCA and the squared r-phi DCA. The pointing resolution in r-phi and Z directions can be calculated with the full STAR detector simulation based on the design parameters, as-built dimensions, and from the results of surveys of the sensor ladders.

The instrument must be capable of a single-track reconstruction efficiency in a Au+Au collision environment of better than 60% for pions at 1 GeV/c that are emitted from the center of the detector within a rapidity window of ± 1 unit. This efficiency is defined as the fraction of TPC tracks that have a correct association to PIXEL hits on both layers and that has at least one hit in the IST and/or SSD layers. The single-track efficiency will be calculated using the full STAR simulations package with input taken from the design parameters and as-built dimensions of the detector.

The STAR DAQ1000 system allows reading out events that include the TPC with a dead time of no less than 4% at 1 kHz. The HFT should not add significant dead time to this value. The threshold value is completely driven by the existing non-replaceable components on the sensor modules on the ladders of the SSD.

The Simulation and Data analysis environment and methods

Of the three high level KPP requirements, the third one, namely the overall system dead time, is a direct measurement during data-taking in runs with the HFT detector included in the data stream. The remaining two require the presence of a working reconstruction chain and an appropriate data sample (real or simulated).

The first KPP, i.e. the pointing resolution of the HFT system in the R-ϕ [XY] and Z directions is an observable and can be determined either by simulations or real data (if available). Even though the use of real data was a desired, but not required,

condition, we are in a position to demonstrate the satisfaction of this KPP with both simulations and real data. This was possible mainly due to the precise metrology and precise alignment of the PXL and IST detector elements using data from a cosmic run that preceded the Run-14 data taking.

The second KPP is not an observable and requires the use of detailed simulations of the full system.

Detector Modeling in Simulations

It was explicitly requested that all simulations should include both a detailed description of the as-built HFT system and a collision (i.e. tracking) environment that closely represents the collider conditions. We used a very detailed modeling of the material and geometry of the HFT subsystem elements to satisfy the first implicit condition for simulations.

For the PXL detector, a detailed account of all materials, composition and amounts, was recorded during construction and corresponding updates were done in the simulation engines (GEANT). Attention was paid to properly model the shape and density of all materials, whether active (sensors) or inactive (support structures, cables etc.) in sufficiently high granularity based on actual SolidWorks[1] models of the detector. The same detailed modeling was done for the two intermediate trackers, the IST and SSD.

There is one difference between the PXL detector, as installed, and the PXL simulation model. The actual detector was built with copper-traces cables in all outer ladders and in eight out of ten inner ladders. Two of the inner ladders were equipped with aluminum-traces cables which results in about 0.10% X_0 less in overall radiation thickness. In simulations we used everywhere the copper-traces cables.

Figure 1 shows a partial view of the three subsystems of HFT (cables and other support material are not shown for clarity). One sees in magenta color the innermost (PXL) detector surrounding the beam pipe followed by the IST (yellow-blue) and the SSD (red-green-blue). The detailed modeling of the HFT system is apparent.

Spyridon M
Deleted: *I*

[1] 3D CAD modeling package

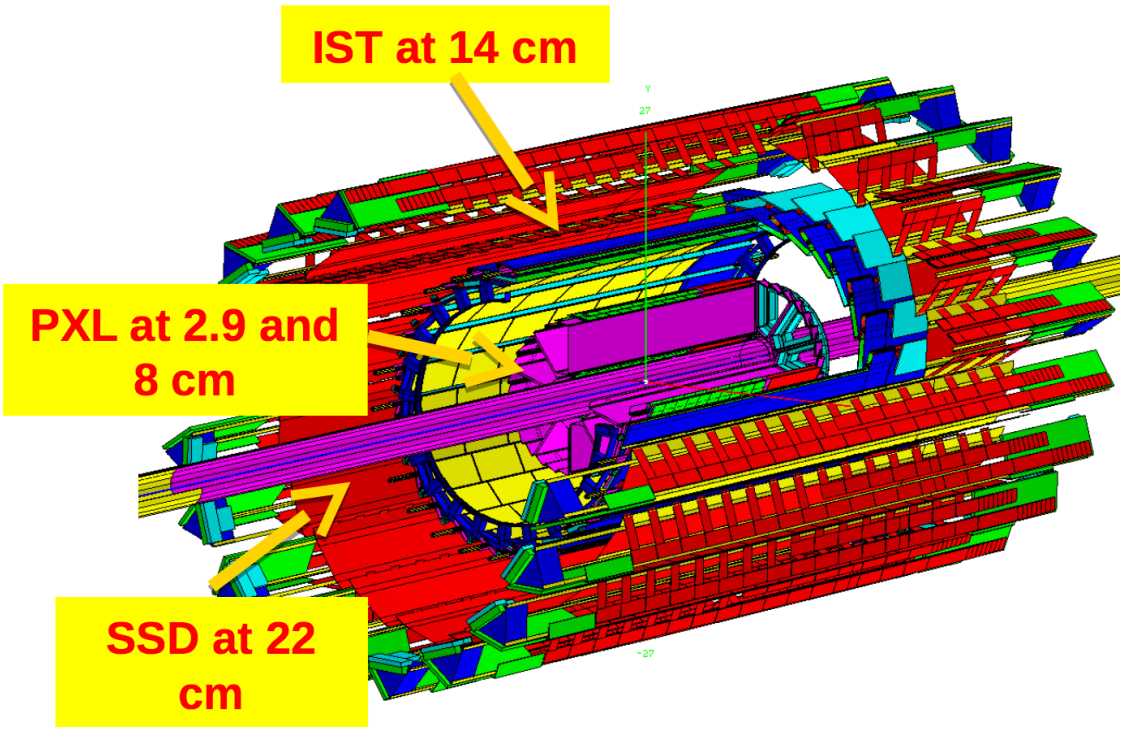

Figure 1 : An overall view of the HFT model in GEANT showing the detailed modeling of each subsystem. In this view, several objects of the model like cables and support structures are not shown for clarity.

The Collision Environment – Pileup and Embedding

To address the second condition, that of a realistic collision (i.e. tracking) environment, we used two separate approaches. In the first one, fully simulated Au+Au collisions were mixed with "background" at the detector hit level. The background sources differ for each detector; they are negligible for the IST (and SSD) systems but very important for the PXL system (mainly due to its proximity to the collision point and its relatively long sampling time of 185 μs). For PXL, the two sources of background hits are i) out of time, non-triggered collisions falling into the same readout time-frame as the triggered event and, ii) electron-positron pairs created in electromagnetic interactions between beam particles (from now on called UPC electrons). Both sources were carefully estimated and included in our simulations. We collectively call them ***pileup***. It is worth mentioning at this point that by comparing PXL hits densities from real data to estimated ones [see *Figure 10* and *Figure 11*] we validated the correctness of the latter.

We also used an alternative method called ***embedding*** in order to best represent the collision environment. In this method, real data events are used as background and a few simulated tracks of the species of interest are embedded in them for subsequent tracking and efficiency analysis. The embedding can be done at the raw

Spyridon M
Deleted:
Spyridon M
Deleted:

pixel level or at the hit level; we were able to perform the latter one for the needs of this report but for the PXL detector we expect no difference, as overlap of hit clusters in PXL is virtually zero due to the fine granularity of this detector.

Below we present results from fully simulated events with pileup since the STAR environment cannot yet deal with embedding for high-resolution vertex detectors.

The Offline Reconstruction Chain

We processed the data using a so-called "Fast Offline" reconstruction chain, meaning that the detector systems of interest (TOF, TPC, IST, PXL plus the trigger detectors) are not fine-tuned and optimized in their calibrations and performance. Examples include their relative alignment, the TPC calibrations, TOF timing, IST gains and also the IST and PXL masking of noisy channels.

At the same time the offline codes used for reconstruction, e.g. tracker and vertex finders, were also not tuned and optimized in their performance, as this is the first time that such a high precision detector is included in the reconstruction chain. It is therefore fair to say that our un-tuned results set a lower limit in the system's performance.

Figure 2 shows the transverse (X-Y) [left panel] and (X-Z) [right panel] position of the reconstructed triggered event vertex in the event sample we used for this analysis. The beam spot almost coincides with the origin of our global reference system in STAR. One also sees that almost all vertices lie within a couple of hundred microns from the beam center and at Z-positions -6 < Z_V < 6 cm. The two arrows in the right panel show the acceptance cut we used in our analysis of |Z_V| < 5 cm.

Spyridon M
Deleted:

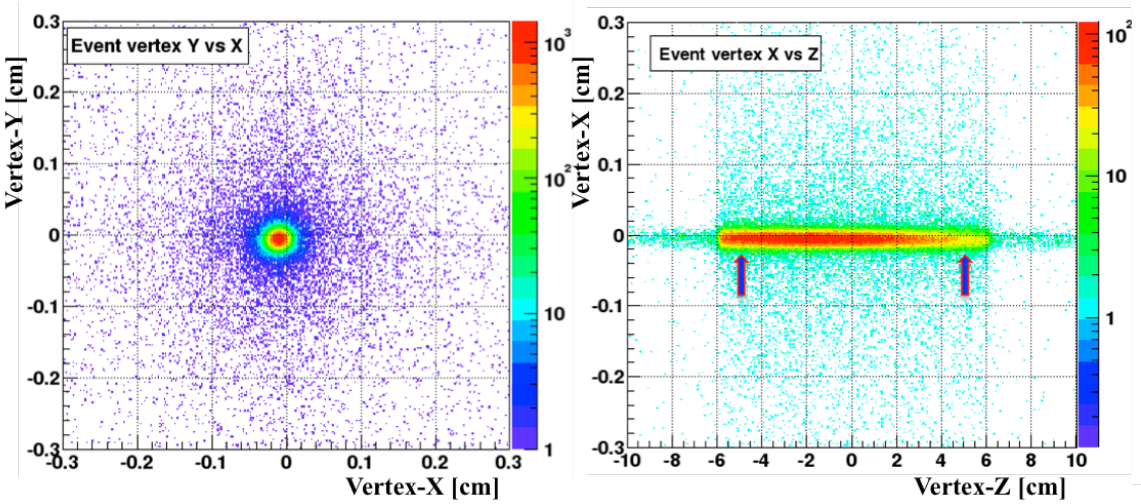

Figure 2 : The event vertex X-Y position [left panel] and X-Z position [right panel] for all triggered vertices in the data sample used for this analysis. The beam spot is almost at the origin of our global reference

system. The arrows in the right panel show the cut in the vertex position of $|Z_V| < 5$ cm that is applied in the analysis.

The Alignment of PXL and IST detectors

The internal pixel alignment within the PXL sector, and sensor alignment the IST and SSD ladders was done with survey measurements. The PXL survey measurement was conducted via a Coordinate Measurement Machine (CMM) with a reproducibility of <20 μm for any pixel position within the single sector. The sector-to-half position was also measured with a precision and reproducibility of <10 μm. The relative alignment between two PXL halves and the refinement of the relative alignment between individual sectors have to be done with physics tracks after the detector is installed in STAR.

We carried out the preliminary internal alignment calibration for the PXL and IST system using the zero field cosmic ray data collected on Feb. 6-9, 2014. The basic idea is to use the two high-precision hits from two layers on the single PXL sector and perform a straight-line projection to align the PXL sector in the opposite direction as well as the IST ladders. The background level is extremely low in the cosmic ray events and the tracks typically have relatively large momentum (> 1 GeV/c) so that the resolution impact due to multiple Coulomb scattering is minimal.

Figure 3 shows the residual distributions between the measured hit positions with respect to the straight line projection in three dimensions for hits at inner and outer ladders, respectively. The grey and blue histograms show the distributions before and after the alignment, respectively. The inserted numbers show the mean positions and the widths from Gaussian function fits. The widths from the fits to the inner and outer distributions after the alignment well match the expectations considering both contributions from the PXL hit resolution and multiple Coulomb scattering.

Spyridon M
Deleted: *I*

With the same method, we also did the alignment between the IST ladders w.r.t. the PXL detector. *Figure 4* shows the IST residual distributions w.r.t the straight-line projection from the PXL hits in the same side and opposite side respectively. The resolution in the Z direction is much broader than in X, Y due to the IST pad dimension (6 mm) in this direction.

Spyridon M
Deleted: *I*

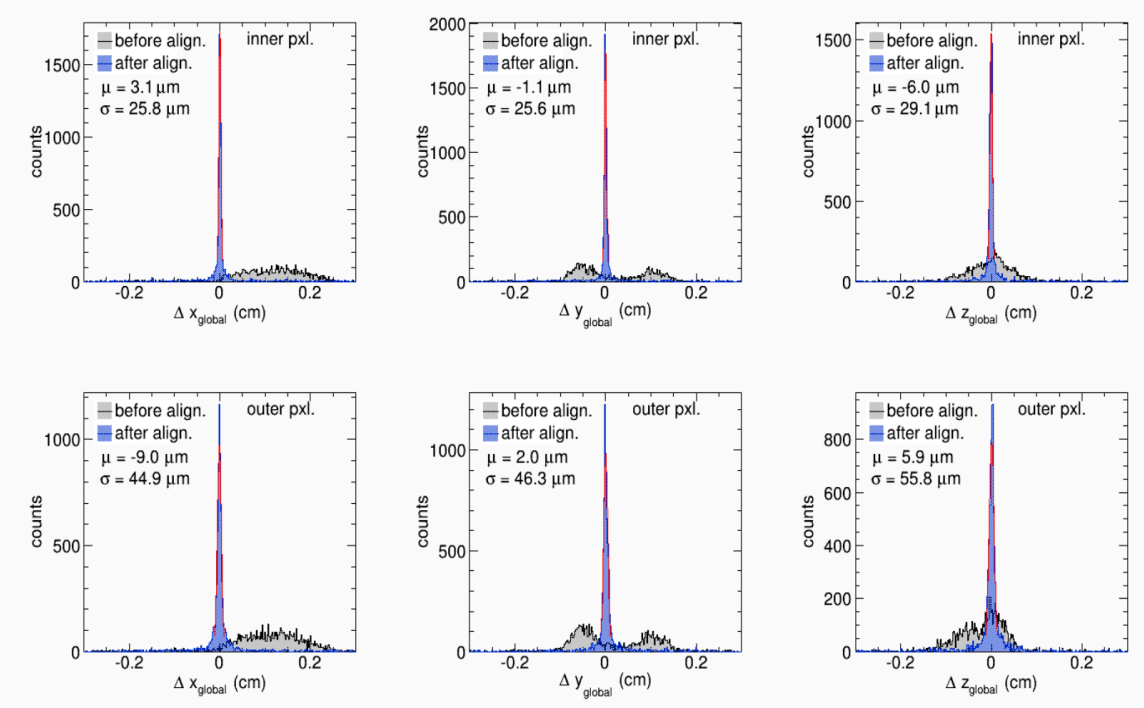

Figure 3 : PXL self-alignment using cosmic data tracks. The grey (blue) distribution show the hit residuals in X,Y,Z before (after) the alignment

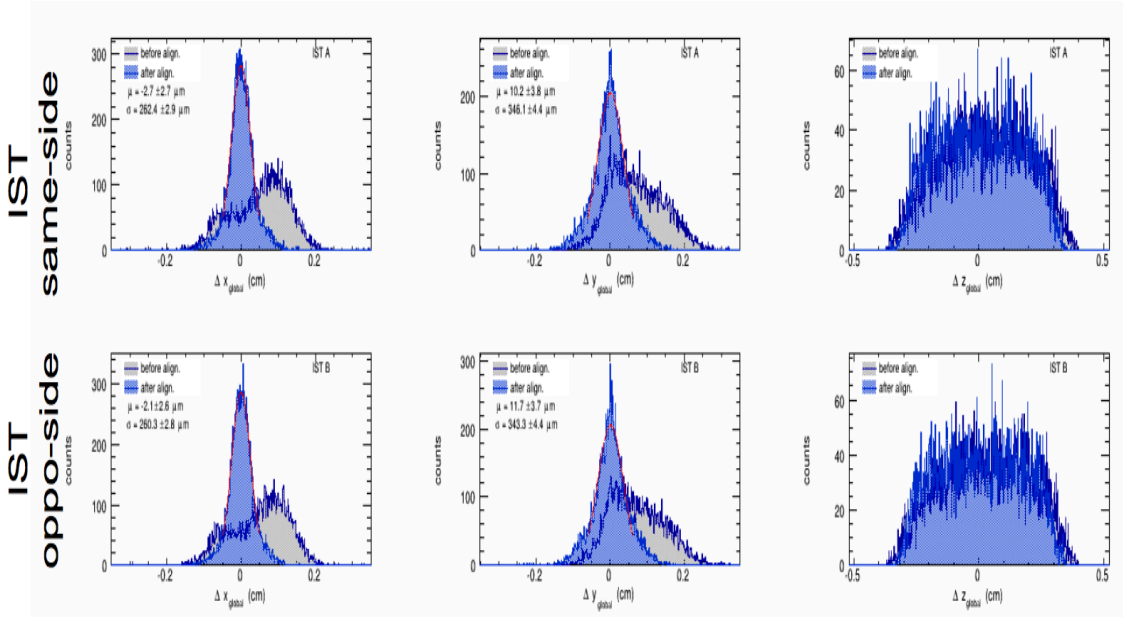

Figure 4 : IST alignment relative to PXL detector. The grey (blue) distribution show the hit residuals in X,Y,Z before (after) the alignment. The broader distribution in Z-coordinate is due to the IST padlength in in that direction.

Results

All results presented in the following sections are obtained either from triggered events (Data) or simulated collisions (as stated) where the beam-direction position of the event vertex (V_Z) is reconstructed within $|V_Z| < 5$ cm from the geometrical center of the PXL detector (which roughly coincides with the global reference system of the STAR detector). This is to avoid acceptance effects at the edges of the detector. Also for the sake of uniformity, all results are shown in the pseudo-rapidity range of $|\eta| <= 0.5$ and this is to avoid geometrical acceptance effects around the edges of the detectors. To make sure that the reconstructed tracks in the TPC are of good quality, we require that each accepted track has at least 20 (of the possible 45) reconstructed hits assigned to it by the tracking program.

All results are including the PXL and IST subsystems in the data taking and tracking. The SSD material is included in all analyses but its hits were not included in tracking.

KPP-1: DCA resolution of HFT system

We present results on DCA resolution using both data from Run-14 and simulations. The pointing accuracy of a vertex detector is typically characterized by a quantity called DCA that is defined as the Distance of a track to the event vertex at its point of Closest Approach. This three-dimensional quantity we call DCA_{3D} while its projections in the bending (r-phi) and non-bending (r-z) plane are labeled DCA-XY and DCA-Z respectively. This pointing is applicable and relevant only for tracks originating at the event vertex. We call them primary tracks as opposed to global tracks which are all TPC tracks reconstructed in the event. A global track becomes primary after it satisfies proximity criteria to event vertex and the constrained fit to the event-vertex point is successful. Primary tracks by definition have near zero DCA therefore the DCA information is taken from its global track copy properly propagated to the DCA point with respect to the event vertex.

The Event vertex position itself is not an observable but it is typically estimated at the point where the sum of the weighted distances from a track sample is minimum, therefore the position of the event vertex is approximately true and an error is assigned to its estimated position coordinates by the fitting program. The event vertex position error, together with residual misalignment errors, will be quadratically added to the observed DCA values, and therefore there is a need to keep them at negligible levels. This is achieved i) by keeping misalignments below or around 20 microns (as we discussed above) and ii) by using high multiplicity central Au+Au collisions where the estimated event vertex error is within or around 10 microns [see also *Figure 12*] (the error is inversely proportional to the square root of the number of tracks used in the vertex determination).

Spyridon M
Deleted: /

Figure 5 and *Figure 6* show the selection of identified particles in the data sample. To select kaons for the required DCA resolution plots, we used both Time-Of-Flight (TOF) information and Ionization energy loss (dE/dx) in the TPC. *Figure 5* shows the 1/β [left panel] and dE/dx [right panel] track information as a function of the track momentum. Starting with the proton band (higher TOF and dE/dx values) we also see the kaon and pion bands. Clearly the discriminating power of the TOF information is much higher that the dE/dx in the momentum range of interest (750 MeV/c) as shown by the blue arrows in the graphs.

Figure 6 shows the combined power of both the TOF (shown as calculated mass squared (m^2) for each track) versus the dE/dx for two momentum ranges. The left panel of the figure shows the PID discrimination over the full range of momenta where we show DCA resolution results in *Figure 9* [0.1 – 1.5 GeV/c] whereas the right panel shows the same PID separation in the critical momentum range around the 750 MeV/c value [0.7 – 0.8 GeV/c]. The three species separation is shown as three horizontal bands at their expected m^2 values in $[GeV/c^2]^2$ of 0.938^2 for protons, 0.493^2 for kaons and 0.139^2 for pions. It is apparent that simple m^2 cuts would yield very high purity samples for each species for further DCA resolution analysis. The cut values we used in our analysis are shown by the red arrows.

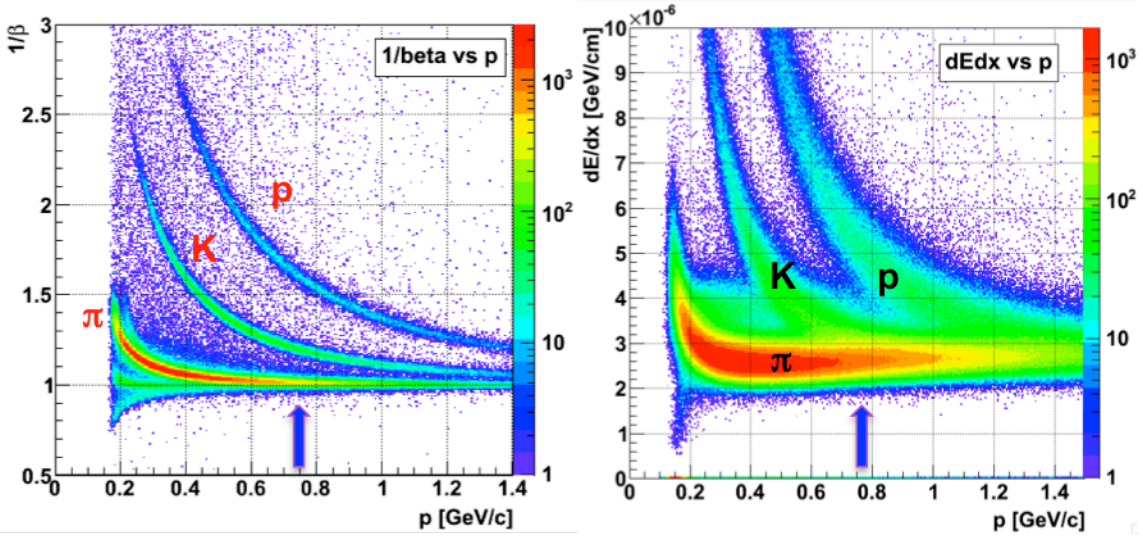

Figure 5 : TOF [left panel] and dE/dx [right panel] as a function of momentum. Starting from top we see the three major bands for protons, kaons and pions. The arrows show the location of the 750 MeV/c point where we see that the TOF has greater discriminating power.

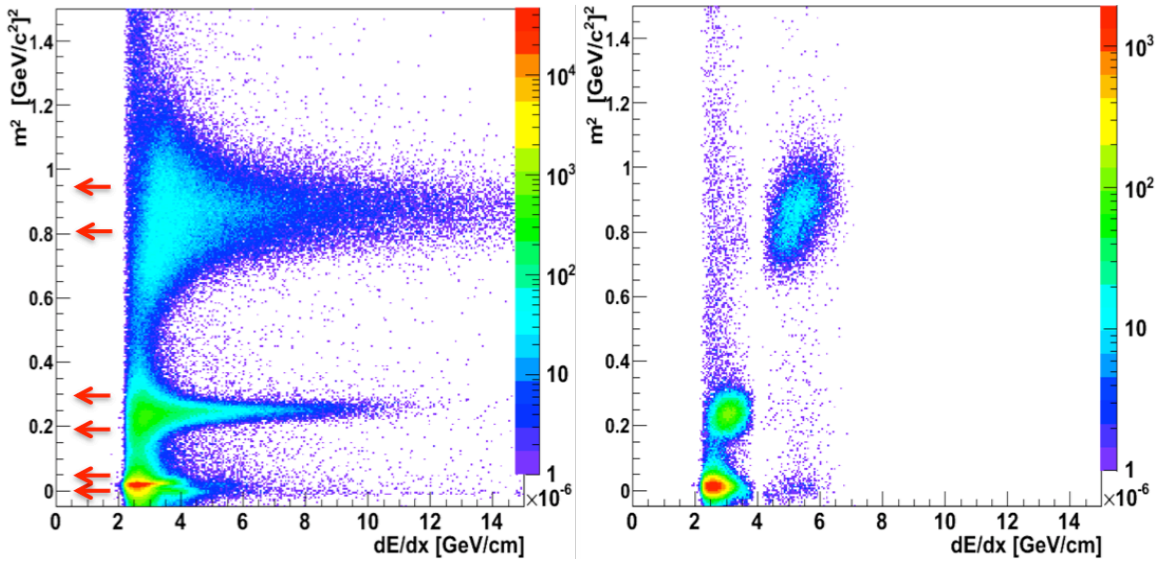

Figure 6 : Kaon selection using the combined TOF [m²] and dE/dx information for two momentum ranges [0.1-1.5 GeV/c] (left panel) and [0.7-0.8 GeV/c] (right panel). Starting from the top the three major horizontal bands are protons, kaons and pions at their expected m² values of 0.938², 0.493² and 0.139² [GeV/c²]² respectively. In both panels, a dE/dx cut of two sigma around the expected value was applied. The arrows show the applied m² cut-ranges in order to obtain a clean sample for each species.

Figure 7 [left panel] shows the raw, per track, DCA-XY distribution as a function of the reconstructed track momentum for all hadrons (no-PID selection). We observe that the distribution is nicely centered on zero for all momenta. The right panel of the same figure shows the DCA-XY distribution (y-axis projection) of the momentum slice around the value of interest, between 0.7 and 0.8 GeV/c. We see that the distribution is a Gaussian with a small amount of outliers. The raw fit to this sample returned the value of 58 μm but a double Gaussian fit, to reject the outliers, returned the value of 46 μm for the central peak.

Spyridon M
Deleted: *

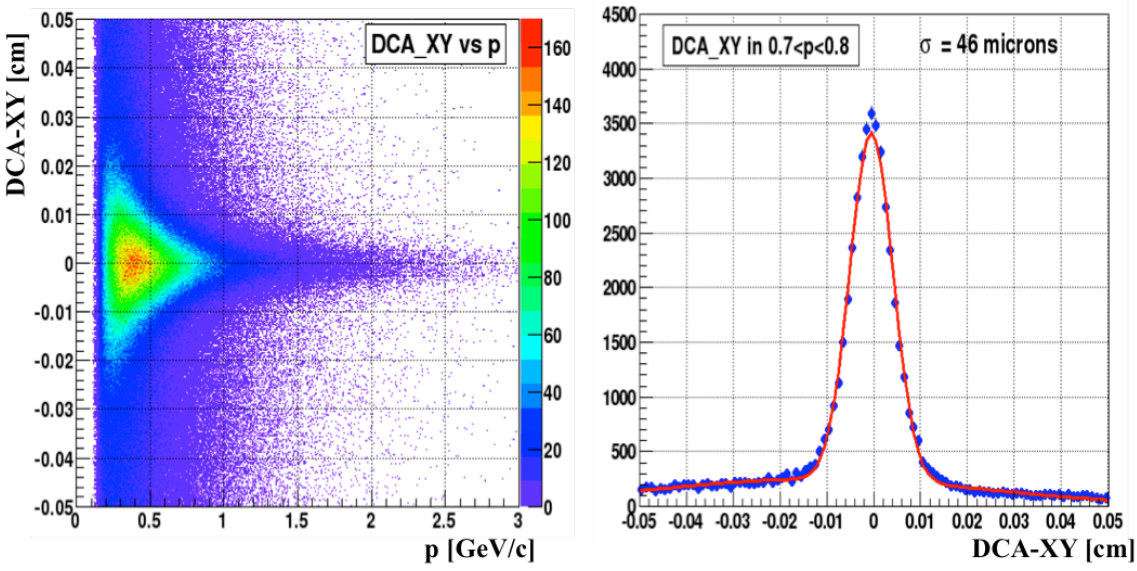

Figure 7 : (left panel) DCA-XY raw, per track, values as a function of momentum. (right panel) DCA-XY distribution in the momentum range 0.7 < p < 0.8 GeV/c. The red line is a double Gaussian fit to the data points.

Figure 8 shows the average DCA-XY resolution for tracks with momenta greater than 0.5 GeV/c as a function of the azimuthal angle in degrees for all hadrons. The red dashed lines show the approximate location of the sector walls. According to our conventions, the first PXL sector is located in the angular range of 90 to 126 [90+360/10] degrees; the third vertical red-dashed line from the right marks this position. We see that the distribution is rather flat with most points contained in the 50-60 microns band. In general, the bins before or including a wall boundary have a larger DCA value than the ones following, since more material is "seen" by the tracks. Two of the inner ladders out of ten sectors of the Run-14 PXL detector were constructed using low mass aluminum traces in the cables (optimal configuration) while the rest were constructed using copper cables. The location of these two sectors (sector six and seven) is shown in the figure by the two blue arrows. We observe that the average DCA value in these two sectors for this momentum range is lower than the average values in the other sectors.

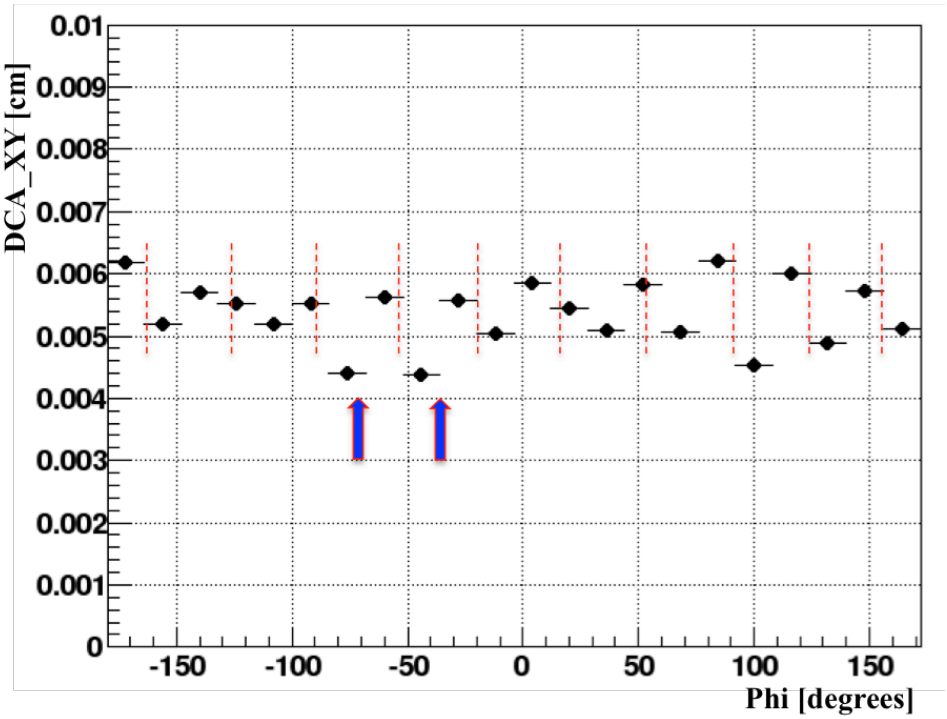

Figure 8 : DCA vs phi for p>0.5 GeV/c. The blue arrows show the location of the two PXL ladders (6 and 7) that were constructed with aluminum traces in the readout cables instead of copper traces. The red dashed lines show the approximate location of the sector walls.

Figure 9 shows the DCA results in the XY [upper row] and Z [lower row] directions for data [left column] and simulations [right column]. The different sets of color points represent the pions, kaons and protons based on the event generator

Spyridon M
Deleted: I

Spyridon M
Deleted: I

information for the simulations and the PID analysis for the data as we discussed above.

We observe that both XY and Z distributions show a remarkable agreement in shape and scale between Data and Simulations; large DCA values at low momenta due to material scattering and small values at larger momenta, approaching values around 30 microns. In the critical value of 0.750 GeV/c shown by the arrows, the kaon band is clearly below the threshold value of 60 microns in both data and full system simulations.

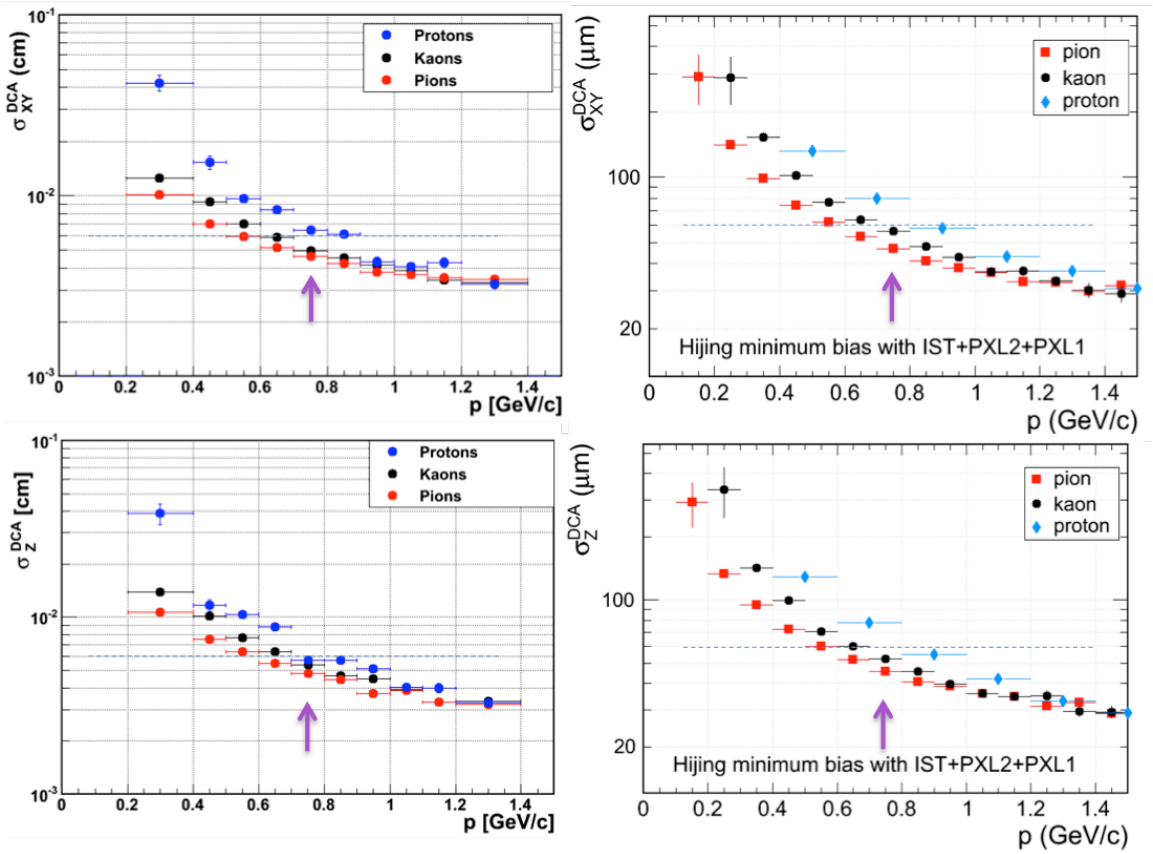

Figure 9 : DCA resolution results as a function of momentum for Data [left column] and Simulations [right column]. The upper row shows the DCA-XY and lower row the DCA-Z results.

We should keep in mind that these results averaged over all azimuthal angles are from data that are not fully calibrated and optimized. They also represent the performance of the "thick" version of the PXL detector, the one with the copper-traces cables. It is reasonable to expect that the "thin" aluminum cable system will exhibit performance near the optimal KPP value of 45 microns for 0.750GeV/c kaons.

KPP-2: Single-track Reconstruction Efficiency for 1 GeV/c pions with the HFT in tracking

Single pion reconstruction efficiency is calculated by simulating the input Monte Carlo (MC) charged pion tracks into a realistic Au+Au collision environment. The track reconstruction efficiency with the HFT system is defined as the probability of reconstructing the track with at least two correct (reconstructed hits should be those that are really induced by the corresponding MC input track) hits in the two PXL layers and at least one correct hit in the IST layer for a good reconstructed TPC track. The efficiency includes the track-hit finding efficiency as well as the hit loss due to other contaminated hits.

In this approach, we run the full Hijing events through the GEANT simulation with the expected pile-up PXL hits included, and then process them through the STAR standard simulator and offline reconstruction chain.

a) Pile-up hits in the PXL detector

The integration time of the PXL detector is about 187 μs. At normal RHIC Au+Au 200 GeV running, a single PXL event may contain hits from multiple collisions including those from the triggered event, the pile-up events from different crossing bunches, and the low momentum electrons from ultra-peripheral collisions. To have a realistic estimation of the tracking efficiency with the HFT, in our simulation, we embed additional hits according to the expected hit density based on the RHIC collision luminosity and the UPC electron production rate.

To estimate the hit densities at each PXL layer due to the pile-up Minimum Bias collisions, we processed through GEANT Minimum Bias Hijing events distributed along the beam axis using a Gaussian distribution with the width of 40 cm, comparable to what we observed in Run14 data. Then we combined the PXL hits generated in GEANT simulation from ~10 Minimum Bias events which corresponds to ~50 kHz Au+Au collision rate. For the background hits due to the Ultra Peripheral Collisions (UPC) electrons, we used the STARlight event generator and then propagated the UPC electrons in the STAR GEANT to simulate the real detector effect. The additional contribution due to the spiral trajectories of the very low p_T electrons in the 0.5 T magnetic field introduces another 20-30% increase in the observed hits in the first PXL layer.

The following table lists the calculated hit densities from different sources in the first and second PXL layer (PXL1 and PXL2)

	PXL1 – inner layer	PXL2 – outer layer
Radius	2.9 cm	8 cm
Integrated MB collisions	5.6 cm^{-2}	2.2 cm^{-2}
UPC electrons	21.0 cm^{-2}	3.0 cm^{-2}

Total pile-up hits	26.6 cm^{-2}	5.2 cm^{-2}

b) Pile-up hits in PXL detector were loaded when we processed our signal event simulation using the Hijing generator.

Monte Carlo events with the vertex Z position were required to be within |Vz| < 5cm and tracking was carried out with the STAR tracking software (Sti) with the latest geometry implementation. The vertex finding in Au+Au collisions followed the standard Minuit 3D vertex finding and fitting.

Figure 10 shows the correlation between the total number of TPC tracks with the number of HFT hits on each layer. One can clearly see the offsets in the number of PXL hits at vanishing number of TPC tracks. These correspond to the background hits from pileup Minimum Bias events and UPC electrons that were added in the simulation. The correlation showing multiple strips is because there were finite pile-up input files and each strip corresponds to a production set using the same pile-up input file.

Spyridon M
Deleted: I

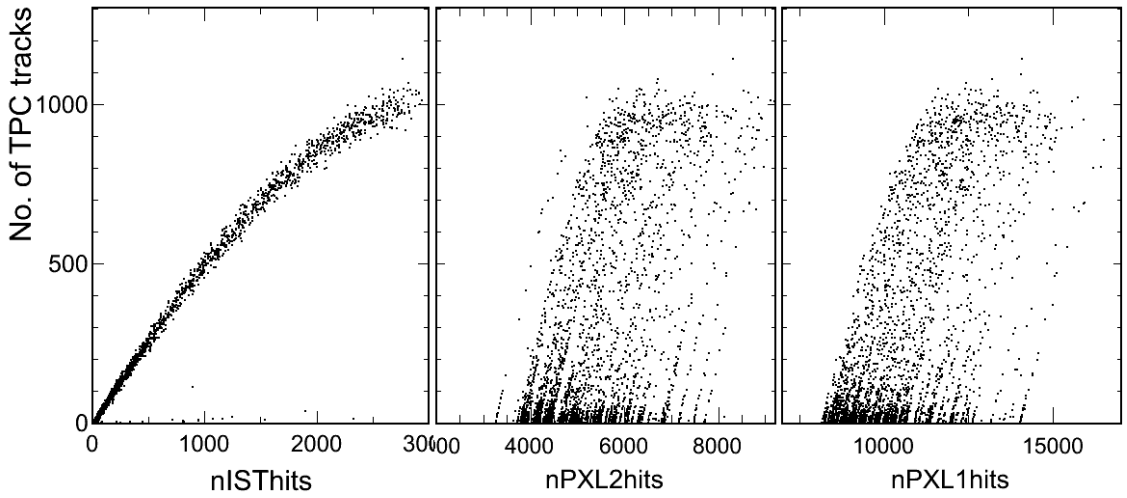

Figure 10 : Correlation of the reconstructed TPC tracks vs. the number of reconstructed HFT hits in each layer from Hijing simulations. Background hits from pileup Minimum Bias events and UPC electrons are included in the PXL hits.

The hit distributions in the different layers were extracted from typical Au+Au 200 GeV collisions with the raw ZDC coincidence rate of ~50 kHz and the vertex Z position within |Vz| < 5 cm. *Figure 11* shows the number of reconstructed TPC global tracks within |η| < 1 vs. the number of PXL and IST hits at each layer from the minimum bias collisions from real data. The offsets seen in the PXL2 and PXL1 layer with vanishing number of TPC tracks show a comparable level as used in our Hijing simulation in the previous section.

Spyridon M
Deleted: I

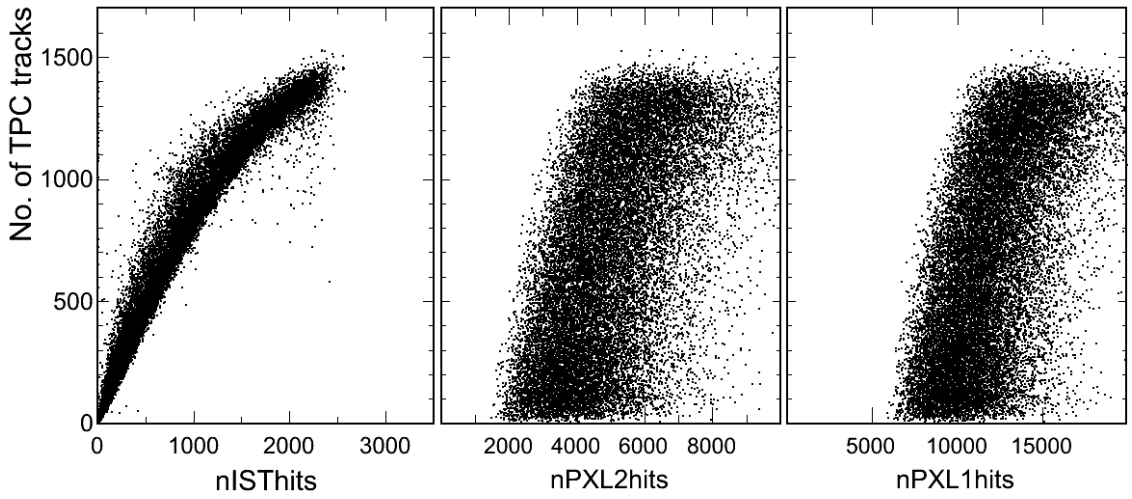

Figure 11 : Correlation of the reconstructed TPC tracks vs. the numbers of reconstructed HFT hits in each layer from real Au+Au data at a ZDC rate of 50 kHz.

Figure 12 shows the primary vertex resolution vs. TPC track multiplicity from simulated minimum bias Au+Au Hijing events. The resolution is calculated as the quadratic sum of resolutions in all three dimensions. The solid line depicts a fit with the functional form $a/\sqrt{N} \oplus b$.

Spyridon M
Deleted: *I*

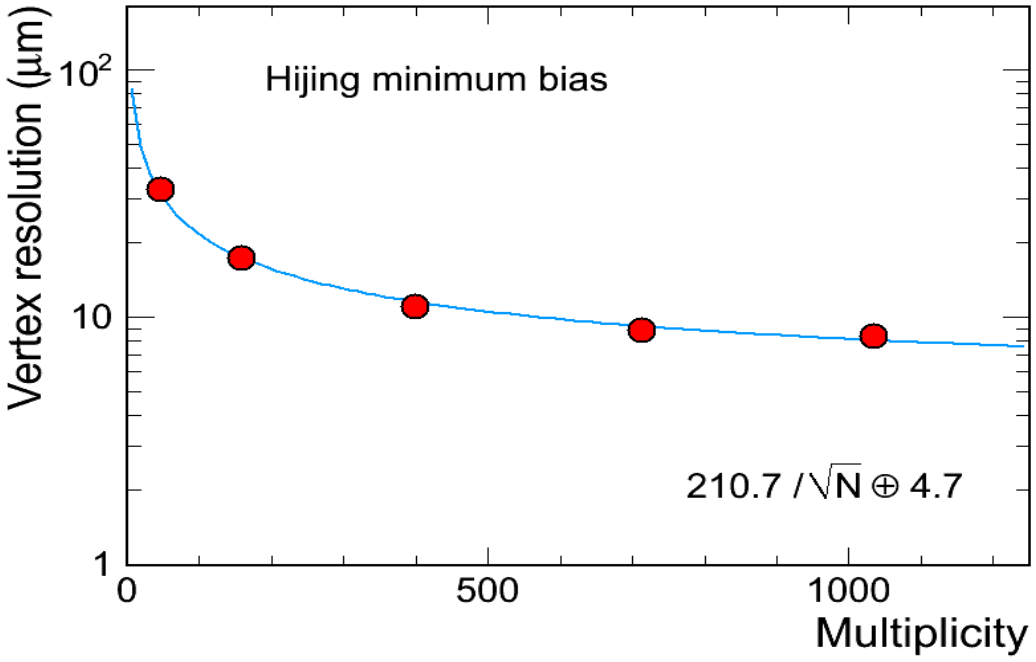

Figure 12 : Primary vertex resolution (quadratic sum of resolutions in all three dimensions) of Hijing simulation events vs. event multiplicity from the standard STAR Minuit vertex finder. The solid line depicts a fit with the functional form $a/\sqrt{N} \oplus b$.

Figure 13 presents the PXL+IST tracking efficiency vs. p_T for charged pions from Hijing minimum bias simulations with the PXL pileup hits included. The efficiency is defined as the tracking efficiency for a good TPC track to pick up hits in both PXL layers and at least one hit in the IST layer. The open circles show the efficiency for all associations, while the red circles require at least one correct association in all three layers. One can see the single pion efficiency at 1 GeV/c is >65% in the Au+Au collision environment. This satisfies the CD4 KPP threshold of > 60%.

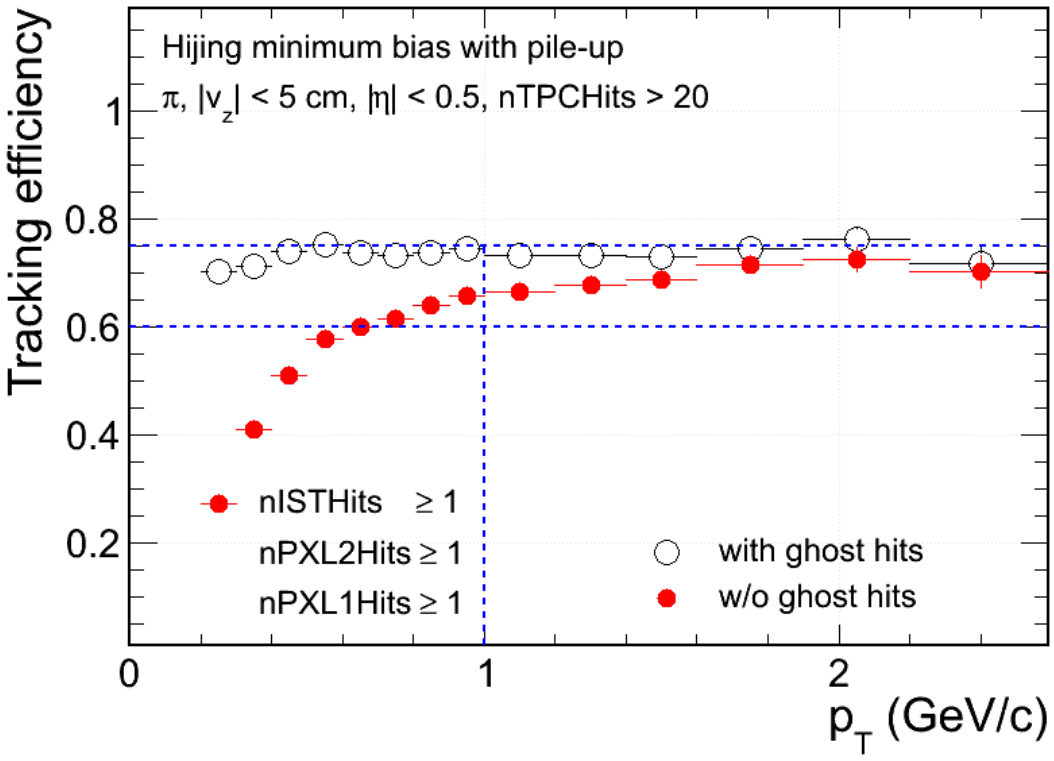

Figure 13 : Single-track reconstruction efficiency as a function of track transverse momentum (p_T) for pions in minimum bias Au+Au collisions at 200 GeV. The HFT tracking efficiency is shown for all associations (open circles) and correct associations (solid circles).

KPP-3 Compatibility with STAR DAQ 1000

The compatibility with STAR DAQ 1000 is confirmed by observing the behavior in real data taking with the full STAR detector and with beam.

Several dedicated runs were taken to investigate and document the dead time achieved when running the HFT system together with the rest of STAR. The triggers were designed to read out the full HFT (SSD+IST+PXL). The result is shown in Figure 15 which is a snapshot of the STAR DAQ monitor. Since the dead

times are OR'ed after triggering, the PXL and IST do not add to the TPX (i.e. readout system for TPC). The SSD does add to the total dead time of the system.

Det	State	Dead	CPU%	Evts	Hz	kB/s	Err
TOF	RUNNING	3 %	14	366886	989	3948	0
BTOW	RUNNING	2 %	13	367156	1001	9808	0
Trigger	RUNNING	0 %	0	367041	1003	3654	0
ETOW	RUNNING	2 %	13	366533	975	2049	0
BSMD	RUNNING	0 %	13	0	0	0	0
ESMD	RUNNING	2 %	51	366698	980	18184	0
TPX	RUNNING	4 %	25	367453	1005	250738	0
PXL	RUNNING	4 %	15	367423	1002	55893	0
MTD	RUNNING	2 %	13	367230	1005	980	0
IST	RUNNING	4 %	60	367329	1002	13665	0
SST	RUNNING	20 %	16	367429	1001	87062	0
GMT	RUNNING	0 %	13	0	0	0	0
L4	RUNNING	0 %	0	-1/0	0	0	0

Figure 14: Screen shot of the STAR DAQ monitor showing the detector system, the recorded dead time, and the event rate recorded to tape (Hz). The requested trigger rate was 1250 Hz while the event rate to tape was approximately 1000 Hz for all systems, principally due to the dead time in the SSD.

A sequence of measurements was also done to map out the performance of the HFT DAQ system vs. trigger rate. **Error! Reference source not found.** shows the dead-times for PXL, IST, SSD, and TPX vs. the requested trigger rate. These results were recorded after the inclusion of SSD in June and during the ^{3}He+Au run. The TPC (TPX) has a fundamental 45 μs busy to protect the readout of all of the TPC data. This is indicated in the graph with the red dashed line. The dead times for PXL and IST are at or below the TPX dead time, so NO additional dead time is imposed on readout due to inclusion of these two detectors. The hybrids on the SSD ladders (the parts of the ladder that could not be replaced) have an intrinsic busy of 160 μs, so the ultimate achievable dead time will be 15% at a requested trigger rate of 1 kHz. The graph shows that the SSD meets the specification to be able to run with the rest of the system with < 20% dead time at 1 kHz and a linearly decreasing amount of dead time at lower rates.
In all the HFT fulfills the requirement to be compatible with the STAR DAQ.

Figure 16 : Dead time as a function of trigger rate.